Coupling dissolved oxygen microsensors measurements and heterogeneous respirometry for monitoring and modeling microbial activity within sulfide-oxidizing biofilms

X. Guimerà[a], M. Mora[b], L. R. López[b], G. Gabriel[c,d], A. D. Dorado[a], J. Lafuente[b], X. Gamisans[a], D. Gabriel[b]

[a]Department of Mining Industrial and ICT Engineering, Universitat Politècnica de Catalunya, Avinguda de les Bases de Manresa 61-73, 08240 Manresa, Spain.

[b]GENOCOV Research Group. Department of Chemical, Biological and Environmental Engineering. Universitat Autònoma de Barcelona. Edifici Q. 08193 Bellaterra, Barcelona, Spain.

[c]Instituto de Microelectrónica de Barcelona, IMB-CNM (CSIC), Esfera UAB, Campus Universitat Autònoma de Barcelona, 08193, Bellaterra, Barcelona, Spain

[d]CIBER de Bioingeniería, Biomateriales y Nanomedicina (CIBER-BBN), 28029 Madrid, Spain

GRAPHICAL ABSTRACT

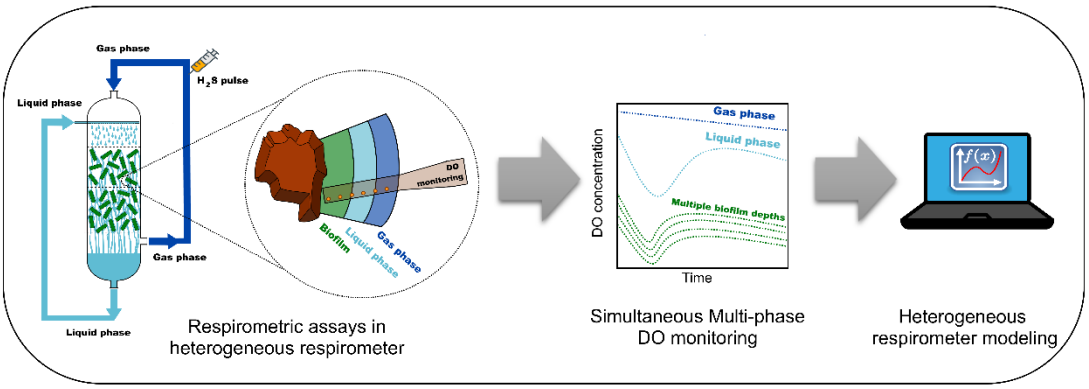

ABSTRACT

A heterogeneous respirometer (HR) was coupled for the first time to a microelectrode monitoring system specifically designed for dissolved oxygen (DO) measuring within the biofilm. Monitoring of the oxygen concentration in the gas and liquid phases was complemented with pioneering monitoring of DO performed simultaneously and continuously at multiple biofilm depths. A set of respirometric tests performed at neutral pH and with initial gas phase concentrations of H_2S ranging from 135 to 6720 ppm_v were

used to assess sulfide-oxidizing activity of a biofilm grown on Pall rings withdrawn from a biogas desulfurizing biotrickling filter. A mechanistic model for the description of multi-step sulfide oxidation within a biotrickling filter was improved considering heterogeneous biomass concentration and biomass activity distribution along the biofilm depth. A comprehensive description of physical, chemical and biological phenomena occurring throughout gas, liquid and biofilm phases resulted in an accurate prediction of system behavior. Model calibration using experimental data estimated a biomass density from 3200 to 4400 g $VSS \cdot L^{-1}$ as well as a decrease in the fraction of active biomass of 0.5, over the 600 μm thick biofilm. Model simulations accurately reproduced experimental respirometric profiles (NRMSE<10%), demonstrating that coupling HR and microelectrodes improved model predictions in comparison to sole gas or liquid phase measurements, thus contributing to a deeper knowledge of biofilms performance in trickled bed biological systems.

KEYWORDS

Heterogeneous respirometry, dissolved oxygen microsensors, biofilm profiling, sulfide-oxidizing biofilm, multiphase reactor modeling.

1. INTRODUCTION

Biodegradation of pollutants contained in waste gases can be efficiently accomplished in biotrickling filters (BTFs), a widespread technology that has been applied for a range of applications from biogas desulfurization to odor removal. The immobilized growth of the bacteria that form the biofilms allows a high transfer area to gaseous contaminants in these configurations and brings additional benefits such as good resistance to operational fluctuations, such as starving periods [1]. Gas-liquid mass transport, diffusion in the biofilm and biological degradation kinetics have been identified as the most relevant processes occurring in a BTF [2]. The inherent complexity of such plug-flow, heterogeneous, multiphase bioreactors requires an accurate characterization of the physical, chemical and biological phenomena taking place, not only to obtain a proper description of liquid and gas phase dynamics, but especially to assess the biofilm behavior in which pollutants biodegradation process takes place.

Although gas and liquid phases can be easily monitored during the biofiltration of gaseous pollutants in BTFs, biofilm performance is difficult to assess since biofilms grow immobilized over the surface of a packing material [3]. In this sense, a more profound knowledge of biofilm dynamics would help improve BTFs design and operability to achieve better performances. To this end, many authors have studied biofilms both microscopically and macroscopically. Some studies characterized biofilm biodegradation mechanisms and activity [4–9], while others placed efforts to describe biofilms development, structure and performance through mathematical modelling [6,10–15].

In gas biofiltration, and also in water treatment, biofilms have been usually modelled through 2D deterministic models that consider biofilms as a planar, stratified phase with constant physical, chemical and biological characteristics where diffusion and biodegradation take place [16,17]. However, some authors have applied novel techniques, such as confocal microscopy and microsensors monitoring to evaluate the internal biofilm structure and processes taking place, highlighting the deep impact of heterogeneity on biofilm properties and performance [18–20]. Up to now, some works have included the effect of biofilm heterogeneity to describe biofilms [21–26]. Nevertheless, improved models based on data from biofilms are still required to avoid inaccuracies between experimental observation and model predictions.

To this end, some adapted respirometric methodologies have been developed for a realistic assessment of the biodegradation activity in biofiltration applications [27,28]. The successful implementation of these methods is mainly due to the simplicity and high sensitivity associated with the monitoring of DO concentration. Bonilla-Blancas et al. [28] developed a heterogeneous respirometry (HR) methodology based on the monitoring of DO concentrations when a pulse of substrate was added to a respirometric vessel mimicking a BTF. The HR was applied to characterize both mass transfer phenomena occurring within gas (G), liquid (L) and biofilm (B) phases, and the biodegradation activity in a trickled-bed colonized by a H_2S-oxidizing biofilm. The HR technique was demonstrated as a powerful tool to characterize biofilms in a multiphase system, under tightly controlled conditions, using experimental oxygen profiles from bulk gas and liquid phases to calibrate a simplified 2D mathematical model. However, their mathematical model predictions could not be calibrated with experimental biofilm profiling since it was not monitored, thus leading to large uncertainties in model estimations. The use of biofilm monitoring tools to obtain experimental data within the biofilm would increase the

reliability of the biological activity characterization and of the mathematical models developed for the description of biofiltration systems description.

Biofilms monitoring using microelectrodes has been performed by several authors reporting successful results. As an example, Zhang and Bishop [9] and De Beer et al. [29] among other authors [24,30–33], studied the biofilm heterogeneity, mass transfer resistance and biological activity using different types of microelectrodes. Nowadays, commercial microsensors, such as Clark-type microelectrodes, are available to monitor biofilms. However, such microelectrodes pose important drawbacks such as their high cost and fragility, and the impossibility of performing simultaneous measurements at multiple biofilm depths. Clark-type microelectrodes do not allow performing multi-point simultaneous dynamic measurements through biofilms, thus being mainly limited to the recording of multi-point, steady-state concentration profiles or to single-point dynamic profiles. During the last years, efforts have been placed to develop different types of microsensors targeting the monitoring of different parameters, such as DO or pH, in one single microsensor with the minimal invasion of the monitored media [34,35]. As an example, an array of gold microelectrodes was developed based on microelectromechanical systems technology to monitor oxygen consumption in aerobic heterotrophic biofilms cultivated in a flat plate bioreactor [36]. This microsensor consisted of an array of eleven microelectrodes distributed in a needle of 1 mm in length. The simultaneous measurement of DO concentration on the eleven microelectrodes allowed the simultaneous evaluation of the oxygen distribution over time within multiple locations in a biofilm. In Guimerà et al. [6], the application of this microsensor to characterize the biofilm allowed estimating the effective diffusivity within the biofilm, in addition to the biokinetics of the microbial culture.

In the current work, a microsensor specifically designed for biofilm monitoring was used in an HR to improve the description of functional and structural characteristics of a sulfide-oxidizing biofilm. To this end, a microsensor multi-electrode design allowing the dynamic and simultaneous multi-point monitoring of DO concentration through several biofilm depths [34] was setup in a HR experimental setup to obtain dynamic DO profiles within a biofilm. In the same way, a mathematical model for the description of H_2S oxidation in a BTF [2] was assessed and modified to describe biofilm as a stratified layer. The suitability of the improved HR to characterize the trickled bed performance, and specially biofilm activity and dynamics, were evaluated by monitoring the oxidation of

H_2S within the HR. The HR was filled with Pall rings, colonized by a H_2S-oxidizing biofilm, obtained from a desulfurizing BTF. The model was calibrated to describe respirometric tests using experimental data from the dynamic evolution of DO concentration within the gas phase and the liquid phase, but also from different points inside the biofilm. Thereby, experimental data obtained under steady-state conditions, and usually used for biofilm models calibration [26,37–40], was replaced herein for experimental data obtained under dynamic conditions in order to increase the reliability of model predictions. Additionally, to the best of authors' knowledge, this is the first time that a microsensor has been successfully implemented for multi-point, biofilm monitoring obtaining relevant data in real-time.

2. MATERIALS AND METHODS

2.1. Heterogeneous respirometer setup

The heterogeneous respirometer setup is shown in Fig. 1a. The respirometer was designed with an easy-to-open system in order to fill the bed volume (0.63 L) with the biofilm-covered packing material to be characterized [41]. The heterogeneous respirometer was manufactured in PVC with a bed diameter and height of 0.059 m and 0.23 m, respectively. The heterogeneous respirometer was prepared to recirculate counter-currently (downflow) the liquid phase, using a peristaltic pump (77200-12, Cole Parmer, USA), and the gas phase, using a gas compressor (Model 3112, Boxer, UK). The system could be operated either as a completely closed system (differential) or as an opened system with respect to the gas phase by shifting the position of the inlet and outlet gas valves (Fig. 1a).

The monitoring of the oxygen concentration in the gas and liquid phases was performed through an O_2 sensor (O_2 SL-sensor, Euro-Gas Management Services, UK) and a galvanic dissolved oxygen sensor (CellOx 325, WTW, Germany), respectively. Both parameters were measured in the gas and liquid recirculation lines. The pH was also monitored (Sentix 82, WTW, Germany) in the liquid reservoir. Both the DO sensor and the pH electrode were connected to a bench-top meter (Inolab Multi 740, WTW, Germany). The pH was also accurately controlled at pH 7.0 ± 0.1 by a high-precision two-channel micro-burette (Multi-burette 2S, Crison, USA) adding either HCl (1M) or NaOH (1M) solutions. Sulfate and thiosulfate concentrations were analyzed by ion

chromatography with conductivity detection using a Dionex ICS2000 (United States) equipment. The system was operated at room temperature (between 20ºC and 25ºC).

2.2. DO microsensor

DO concentration within the biofilm was monitored during respirometric tests using a specifically designed DO microsensor. The DO microsensor was specially designed for biofilm monitoring as described elsewhere [34]. The DO microsensor consisted of a linear array of eleven gold-disk electrodes of 50 µm-diameter and separated by 100 µm, and a rectangular gold one mounted on a minimally invasive micro-fabricated needle (Fig. 1b). Disk electrodes were designed as working electrodes (WE) or sensing electrodes, while the rectangular one was designed as counter-electrode (CE). WE were simultaneously polarized at the oxygen reduction potential [34] (-850 mV) using an 8-channel potentiostat (1010C, CH-Instruments, USA). Electrodes potential was controlled using an external reference electrode (RE) (REF321, Radiometer analytical, France). The electrodes were simultaneously calibrated before biofilm monitoring and the measuring of reduction currents were used to quantify the DO concentration (further information about microsensor preparation and calibration is detailed elsewhere [34]).

Compared to commercial, Clark-type electrodes, the high robustness of the microfabricated needle allowed its utilisation for the trickled bed monitoring. To this end, the microsensor was inserted vertically into the biofilm through the heterogeneous respirometer monitoring port (Fig. 1c) enabling the simultaneous monitoring of DO concentration at 8 different well-defined depths within H_2S-oxidizing biofilm. The dynamic information of the DO concentration evolution within the biofilm, instead of steady-state concentration profiles typically recorded using conventional microsensors, provided a breakthrough approach in the use of HR.

Microsensors suitability for H_2S-oxidizing biofilm monitoring was assessed by quantifying the drift of sensors response during respirometric tests. To this aim, the microsensor response was characterized at the beginning and at the end of each experimental test. Fouling of electrodes over a 4 hour period resulted in a sensitivity decrease lower than 10%, which was a tolerable loss of sensitivity to perform short-term monitoring tests according to Moya et al. [34].

2.3. Performance of respirometric tests in the HR

The biofilm-covered packing material (plastic Pall rings with a diameter of 15.9 mm) was obtained from a biogas desulfurizing BTF, which was operated for more than two years treating an H_2S inlet concentration of 2000 ppm_v [41]. Once the packing material was distributed carefully inside the packed bed container of the heterogeneous respirometer (Fig. 1a, number 6), the microsensor was inserted within the biofilm through the monitoring port. Then, the port was sealed using an epoxy resin. Before starting the respirometric tests, a fresh volume of 126 mL of mineral medium (MM) was added to the HR. The composition of the MM was (g L^{-1}): K_2HPO_4 (0.15), KH_2PO_4 (0.12), NH_4Cl (1), $CaCl_2$ (0.02), $MgSO_4 \cdot 7H_2O$ (0.20) and trace elements solution [42] (1 mL L^{-1}). Additionally, sodium bicarbonate was added as the microbial carbon source to the MM (3.5 g L^{-1} $NaHCO_3$). The MM was continuously recirculated through the colonized packing material for 24 hours with continuous aeration to achieve endogenous conditions, thus ensuring the oxidation of any bioavailable substrates (dissolved sulfide, thiosulfate and/or elemental sulfur) accumulated within the biofilm. Afterwards, the MM was renewed, and the heterogeneous respirometer was operated as a closed system (inlet and outlet liquid or gas flows were not allowed). At this point, the respirometric study was initialized.

Respirometric tests were performed following three basic steps [43]: 1. Calculation of the endogenous oxygen uptake rate (OUR_{end}) from the slope of the DO profile without bioavailable substrates, 2. Re-aeration of the system and 3. Addition of substrate pulses to calculate the exogenous oxygen uptake rates (OUR_{ex}) associated with each substrate concentration tested. In this study, different pulses of pure H_2S were injected in the heterogeneous respirometer to characterize the biofilm (200 μL, 1 mL, 5 mL and 10 mL). The pulses corresponded to initial H_2S gas phase concentrations ranging from 135 to 6720 ppm_v, which is a concentration range commonly found in biogas desulfurization BTFs. After spiking the heterogeneous respirometer with each pulse of the substrate, the system was opened and re-aerated again to reach DO saturation conditions. Gas and liquid phases were recirculated during the respirometric tests at constant flows to set linear velocities of 43.4 and 10.8 m h^{-1}, respectively. During the overall operation, the oxygen concentration was simultaneously monitored in all phases (gas, liquid and biofilm). Experimental data obtained from respirometric tests were used to calibrate the biokinetic and hydrodynamic mathematical model developed to describe H_2S biodegradation in this specific biofilm-covered trickled bed.

2.4. Experimental determinations in the heterogeneous respirometer

Additional experimental analyses were performed to calculate relevant parameters for the mathematical model development. In this sense, the static and dynamic hold-ups, the fractions of the packed bed occupied by liquid, gas, biofilm and packing material, and the biofilm content and biomass fraction in the biofilm were determined following the methodology described in Bonilla-Blancas et al. [28]. Additionally, the amount of biomass attached to the packing support was quantified following the methodology by Lazarova and Manem [30] . In short, once the corresponding assay was finished, the liquid pump was stopped, and the packing material was immediately weighed (W_1). After draining the liquid for a period of 30 minutes, the support was weighed again (W_2). The weight difference between W_2 and W_1 determined the static hold-up that, together with the dynamic hold-up, was used to estimate the volume fraction occupied by the liquid (ε_L^{Bed}). Once drained, the packing material was carefully shaken to withdraw all the biofilm and then was re-suspended in a known volume of water. The clean packing was dried for 12 hours at 50 °C to determine the weight of the support (W_3). The suspended biomass was later centrifuged at 5000 rpm for 10 minutes and the supernatant was discarded to determine the weight of wet biomass (W_4). The volume fraction occupied by the biofilm (ε_B^{Bed}) was calculated by dividing W_4 by the product of wet biofilm density times the volume of the packing material tested. A wet biofilm density of 1.11 g mL^{-1} was used to calculate ε_B^{Bed}. Finally, the wet biomass was dried for 12 hours at 50 °C to determine the dry weight of the biomass (W_5). The volume fraction occupied by the gas (ε_G^{Bed}) in the packed bed was also determined taking into account the space occupied by the abovementioned fractions of the packed bed, including the empty bed fraction of the packing material reported by the manufacturer (352 m^2 m^{-3}).

The fraction of biomass in the biofilm (ε_x) was also determined. It was obtained by analyzing the concentration of total nitrogen in the washed and centrifuged biofilm. The general formula $C_5H_7NO_2$ typically used to represent the composition of biomass [44] was used to convert the concentration of total nitrogen into biomass concentration. Then, the biomass concentration was divided by the total solids concentration (considered as biofilm concentration) to obtain the biomass fraction in the biofilm. Total solids were analyzed following the standard method for wastewater analysis [45]. Total nitrogen was analyzed spectrophotometrically (DR3900, Hach, Spain) using cuvette tests (LCK238, Hach, Spain).

3. MATHEMATICAL MODEL DEVELOPMENT

A three-phase model taking into account the mass balances in the gas and liquid phases and within the biofilm was developed to describe the dynamics in the heterogeneous respirometer considering gas and liquid phase recirculation under counter-current flow pattern. The model includes mathematical expressions for the description of mass transport by advection in both the gas and the liquid phase, mass transfer through the gas-liquid interface, mass transfer at the liquid-biofilm interface, internal mass transport in the biofilm and microbial kinetics within the biofilm. The main assumptions, mass balances and model equations considered in this work to describe H_2S oxidation in the heterogeneous respirometer can be found in the Supplementary Information (section S1.1).

3.1. Modeling mass transfer and mass transport phenomena

Gas-liquid and liquid-biofilm mass transport mechanisms were described using global mass transfer coefficients referred to the liquid phase (K_L) and the biofilm (K_B), respectively, while mass transport within the biofilm was modeled by diffusion according to Fick's Law using a dispersion coefficient (D_B).

Mass transport coefficients were determined using empirical correlations as a function of the operating conditions. K_L for both H_2S and O_2 were determined using the Billet and Schultes correlation [46] (Eq. 1), based on the good agreement with experimental determination on previous modeling studies under similar operating conditions [2,47].

$$K_{L,i}=C_L\cdot\left(\frac{\rho_L\cdot g}{\mu_L}\right)^{1/6}\cdot\left(\frac{D_{L,i}}{d_h}\right)^{1/2}\cdot\left(\frac{u_L}{a_p}\right)^{1/3} \quad (1)$$

Where $K_{L,i}$ is the global mass transfer coefficient for component i (m h^{-1}), C_L is the packing material-specific constant, ρ_L is the liquid density (kg m^{-3}); g is the gravitational constant (m s^{-2}), μ_L is the liquid viscosity (kg m^{-1} s^{-1}), $D_{L,i}$ is the diffusion coefficient in the liquid of species i (m^2 s^{-1}), d_h is the hydraulic diameter of packing material defined by $4\varepsilon/a_p$ (m), u_L is the superficial liquid velocity (m s^{-1}) and a_p is the packing material specific surface area (m^{-1}).

According to Guimerà et al. [6] the effect of hydrodynamic conditions and biofilm density in the calculation of both external (K_B) and internal (D_B) mass transport coefficients were included by using Eq. 2 and Eq. 3, respectively.

$$Sh_i = 0.238 \cdot Re^{0.8} \cdot Sc_i^{0.33} \quad (2)$$

$$D_{r,i} = 0.93 - 0.023 \cdot X_b + 1.2 \cdot 10^{-2} \cdot Re^2 + 1.1 \cdot 10^{-4} \cdot X_b^2 \quad (3)$$

Where Sh_i is the Sherwood number for species *i* defined by $K_{B,i}/(D_{L,i}/L_c)$, L_c is the boundary layer thickness (m), Re is the Reynolds number defined by $(\rho_L \cdot u_L \cdot d_h)/\mu_L$, Sc_i is the Schmidt number for species *i* defined by $\mu_L/(\rho_L \cdot D_{L,i})$, $D_{r,i}$ is the relative dispersion coefficient within the biofilm defined by $D_{B,i}/D_{L,i}$, and X_b is the biofilm density (g VSS L^{-1}).

3.2. Modeling biological and chemical oxidation of sulfur compounds

The biological degradation of H_2S within the biofilm was described through a previous model developed after the characterization of the same H_2S-oxidizing biofilm used in this study [3]. The kinetic model considers that sulfide is partially oxidized to elemental sulfur, which is intracellularly stored by bacteria. Elemental sulfur is partially oxidized to sulfite that, in the presence of sulfide, reacts to form thiosulfate. Once sulfide is completely depleted, elemental sulfur and thiosulfate are oxidized to sulfate, the end product of the biological reactions. Detailed information about the bioprocess stoichiometry and kinetics considered in this study can be found in the Supplementary Information (section S1.3, Fig. S1, and Tables S1 and S2).

3.3. Model implementation: system discretization and parameters estimation

The resolution of the dynamic mass balance equations (Eqs. S1 to S5 in the Supplementary Information) that describe the biological, physical and chemical phenomena taking place in the heterogeneous respirometer was performed by a discretization procedure. In this study, the 2D model of the trickled bed was spatially discretized, resulting in 4 nodes along the height of the bed and 6 nodes along the depth of the biofilm. Detailed information about the resulting equations from the discretization can be found in the Supplementary Information (S1.5).

A sensitivity analysis was performed before the model calibration to determine the influence of selected model parameters variation (±10%) on the relative change of DO

concentration in the liquid phase as model output. Parameters showing higher sensitivities were estimated by fitting the simulated DO concentration profiles to the experimental profiles. The fitting method was based on seeking the minimum value of the objective function. This function was defined as the norm of the differences between the predicted DO concentrations by the mathematical model and the experimental data (Eq. 4), both in the liquid phase and within the biofilm.

$$F_j = \sqrt{\sum_{i=1}^{n} \left[y_{exp\,(ij)} - y_{\theta(ij)} \right]} \quad (4)$$

where F_j is the normalized difference between simulated and experimental DO concentrations at the phase *j*, *n* is the number of experimental measurements, $y_{\theta(i,j)}$ is the simulated DO concentration (mg L^{-1}) at the phase j and instant *i* and $y_{exp(i,j)}$ is the experimental DO concentration (mg L^{-1}) at the phase j and instant *i*. Considering that DO consumption was not observed in the deeper biofilm layers, the phases *j* were defined as liquid recirculation DO concentration and the DO concentration measured in the first 4 layers of biofilm. The *F* function was calculated as the unweighted sum of F_j. Parameters estimation was performed using the MATLAB algorithm based on a multidimensional unconstrained nonlinear minimization (Nedler-Mead).

4. RESULTS AND DISCUSSION

4.1. Assessment of model parameters

Parameters of the mathematical model were classified as follows [2]: physical-chemical properties, mass transport and biokinetic parameters and system specifications. In the present study, physical and chemical parameters were obtained from the literature [48,49]. Mass transport parameters were calculated using Eqs. 1-3, while kinetic and stoichiometric parameters were obtained from Mora et al. [3]. A summary of the physical-chemical properties and biokinetic parameters used in this work are found in the Supplementary Information (Table S3).

Parameters related to system specifications were determined experimentally (Table 1). The packing material used herein showed a liquid retention capacity (ε_L^{Bed}) of 0.06 m^3 liquid m^{-3} of packed bed, which is lower than 0.09 m^3 liquid m^{-3} bed obtained using polyurethane foam or 0.10 m^3 liquid m^{-3} bed using 10 mm pall rings [28]. Moreover, the

packed bed exhibited a higher bed void fraction (0.8 m^3 gas m^{-3} bed) compared to that obtained by [28] (0.7 m^3 gas m^{-3} bed). The liquid fraction in the packed bed (ε_L^{Bed}) is important since it is strongly related to the mass transfer rate. High static hold-ups are found when the liquid is loosely retained inside stagnant regions. The latter diminishes the specific area available for G-L contact and increases the mass transport resistance through molecular diffusion between the liquid and biofilm phases [50]. Thus, a high static hold-up decreases the G-L mass transfer rate in trickled beds. Result obtained herein indicated the existence of efficient distribution of the liquid film in the packed bed given that the static hold-up was 25% lower than the dynamic hold-up. Trejo-Aguilar et al. [50] also reported a positive influence of the liquid fraction on the pollutant elimination capacity at a packed bed void fraction of 0.8 m^3 gas m^{-3} bed associated with a higher wetting efficiency in the packed bed. Although the packing material used in this study had a lower superficial area than the 10 mm Pall ring used in Bonilla-Blancas et al. [28] (a_p of 482 m^2 m^{-3}), a similar biofilm fraction was determined (ε_B^{Bed} of 0.063 m^3 biofilm m^{-3} bed compared to 0.06 m^3 biofilm m^{-3} bed). This result, together with the ε_L^{Bed} and the dynamic hold-up obtained for the packed bed used herein, pointed to a proper and optimal biofilm distribution throughout the packing material.

4.2. Analysis of the respirometric tests performed in the heterogeneous respirometer

Experimental tests performed in the heterogeneous respirometer to study H_2S biological oxidation consisted of spiking the gas phase with a specific volume of H_2S (200 μL, 1 mL, 5 mL and 10 mL), which corresponded to initial gas phase concentrations ranging from 135 to 6720 ppm_v. In Fig. 2a, the overall respirogram recorded is presented. Figures 2b and 2c show specifically the DO and O_2 profiles for the 5 mL H_2S pulse.

During the first part of the experiment (t<1.3h), the endogenous activity was evaluated from the slope of the oxygen concentration and the DO concentration in the gas and liquid phases (Fig. 2a), respectively. The DO concentration profile presented a sharp negative slope indicating that elemental sulfur was still accumulated within the packed bed, and that the endogenous phase was not achieved with the initial starvation period. An initial elemental sulfur concentration within the biofilm of 3.5 g S m^{-3} was determined through mass balance from the monitoring data of the BTF from where the colonized packing

material was extracted, and later incorporated into the model as initial conditions used to simulate the respirometric tests.

Each H_2S pulse (Fig. 2a) was added to the system and the response from both the liquid and gas phases was assessed. Fig. 2a shows that the DO concentration monitoring in the bulk liquid phase has a much higher sensitivity than that of O_2 concentration in the bulk gas phase. The addition of H_2S in the gas phase caused high variations in the DO profile due to the H_2S-oxidizing activity, which indicated that the rate-controlling step was apparently the oxygen transfer from the gas to the liquid phase.

The DO concentration in the biofilm was monitored throughout respirometric tests using the DO microsensor. Results obtained from DO monitoring within the biofilm for pulses from 135 to 6720 ppm_v of H_2S in the gas phase are shown in detail in Supplementary Information (section S1.6). In these results, DO concentration is only presented for 6 biofilm layers despite 8 biofilm depths were monitored since DO concentrations were below the detection limit (L_D of 0.05 mg O_2 L^{-1}) in deeper biofilm layers. Below 600 μm of biofilm depth, the measured concentration was lower than the L_D of the sensor indicating that anaerobic conditions were reached at these depths. Therefore, results obtained from the deepest biofilm layers were excluded from the modelling study.

Sulfate and thiosulfate were also analyzed before and after the addition of each H_2S pulse in the respirometer. The most significant results were observed for the 5 mL (Fig. 2b and 2c) and 10 mL H_2S pulses, where only sulfate was detected. In the first case (addition of 5 mL), 6.55 mg S-H_2S were added and 6.50 mg S-Sulfate were recovered. This result indicates that sulfide was oxidized completely to sulfate without producing any other sulfur compound. In the second case (10 mL), 13.1 mg S-H_2S were added while only 9.68 mg S-Sulfate were recovered as sulfate, thus indicating that elemental sulfur was produced and that the maximum sulfide oxidation capacity was already reached under those conditions.

The DO experimental profiles (both in the liquid phase and within the biofilm) recorded during the endogenous period were used to estimate: the depth of the first biofilm layer (z_{ini}), the packing material constant used in Eq. 1 (C_L) and the decay rate (b_H). These parameters were selected based on the high sensitivity of model outputs to the variation of these three parameters (Table S4). The fitting of the mathematical model

to the experimental profiles (Figure S3) allowed estimating a z_{ini} of $3.069 \cdot 10^{-5}$ m, a C_L of 0.2175 and a b_H of $8.96 \cdot 10^{-6}$ g O_2 g TS^{-1} s^{-1}.

4.3. H_2S oxidation modeling in the trickled bed considering biofilm as a homogeneous layer

As the first approach towards the simulation of H_2S biodegradation in the heterogeneous respirometer, a homogeneous biofilm (both constant density and biological activity) was considered. This is the most common approach in biofiltration using 2D biofilm modeling. Biokinetic parameters, characteristic of the biomass used in this study, were previously characterized in Mora et al. [3]. However, they also reported that kinetic constant describing elemental sulfur oxidation (k_S) (Table S2) depends on the type of sulfur and the sulfur particle shape produced by the specific H_2S-oxidizing bacteria developed in each experimental system. In Mora et al. [3] k_S was estimated as a range instead of as a parameter. For this reason, experimental DO profiles corresponding to period IV were used to estimate k_S value. Finally, the estimated value of biokinetic parameter during model calibration was 0.103 g $S^{1/3} \cdot g^{-1/3}$ VSS. In Fig. 3, experimental and simulated respirometric profiles corresponding to the 5 mL pulse of H_2S are presented. Results obtained showed minimal differences in the evolution of measured oxygen concentration in the gas phase. This trend was expected since biofilm dynamics slightly influence gas-liquid mass transport phenomena of poorly soluble compounds as O_2. Regarding the liquid phase, experimental and simulated DO profiles also showed minor differences, although the predicted DO concentration decay was slightly lower than the experimental one resulting in a higher simulated DO concentration at the steady-state (after 450 s). Within the biofilm, higher differences between experimental and simulated DO profiles were found. Predicted DO profiles presented a high DO decrease as a result of H_2S consumption. As can be observed in Fig. 3b, DO concentration in the more superficial (i.e. first) biofilm layer fell below 1 mg L^{-1}, while experimental DO concentration remained above 3.5 mg L^{-1}. Deviations between experimental and simulated profiles decreased for the first three biofilm layers from the surface after 500 s of monitoring, when H_2S was depleted. On the other hand, unlike experimental results, anaerobic conditions were predicted below 400 μm of biofilm throughout the monitored period.

The comparison between experimental and simulated profiles confirmed that considering a homogeneous structure of biofilm is not adequate for biofilm modeling.

Thus, a realistic description of functional and structural characteristics of biofilm is required in order to accurately predict biofilm dynamics.

4.4. H_2S oxidation modeling in the trickled bed considering biofilm as a heterogeneous layer

The mathematical model describing biological H_2S oxidation in the heterogeneous respirometer was improved considering heterogeneous functional and structural characteristics, such as the biomass density and its active fraction, throughout the biofilm. Biofilm modeling including heterogeneous characteristics was performed using the same model parameters presented both in Table 1 and Table S3.

4.4.1. Heterogeneous biofilm description

Biofilm attached to the packing material was described as a heterogeneous phase considering that some of its properties vary along with its depth. Experimental determinations obtained in previous works highlighted that inner biofilm layers presented a higher cell density but a lower biomass activity [36]. According to these results, a variable biofilm density and active fraction of biomass along the biofilm were included in the model in order to improve the biofilm description. An exponential distribution was considered for both parameters following Eq. 5 and Eq. 6.

$$X_b=\rho_b \cdot e^{c_x \cdot z} \quad (5)$$

$$f_a=e^{-c_a \cdot z} \quad (6)$$

where X_b is the biomass concentration within the biofilm (g VSS L^{-1}); ρ_b is the pre-exponential coefficient for the distribution function of biomass concentration within the biofilm (g VSS L^{-1}); C_x is the exponential coefficient for the distribution function of biomass concentration within the biofilm (m^{-1}); Z is the biofilm depth (m); f_a is the active fraction of biomass within the biofilm; and C_a is the exponential coefficient for the distribution function for the active fraction of biomass within biofilm (m^{-1}). The equation used to define the distribution of biomass concentration within the biofilm (Eq. 5) was developed using an experimental constraint in order to ensure a reliable biofilm description. To this aim, the average biofilm density calculated using Eq. 5 must coincide with the value obtained experimentally following the procedure described in section 2.4.

The heterogeneous modeling approach was implemented by replacing X_b by Eq. 5 in the kinetic equations (Table S2) and by multiplying the kinetic expressions by the active

fraction as described in Eq. 6. The model calibration stage was modified in order to include the estimation of novel parameters (biomass density and active fraction) defined in Eq. 5 and Eq. 6. A sensitivity analysis before model calibration was required in order to assess the influence of mathematical model modifications on its response. The biokinetic parameters characterized in Mora et al. [3] were used again for heterogeneous approach simulation. Considering the influence of H_2S-oxidizing bacteria on elemental sulfur oxidation, the k_S was also included in the calibration step to describe more accurately the biokinetics of the biofilm.

4.4.2. Sensitivity analysis for parameters estimation

Model sensitivity to C_x, C_a and k_s was assessed for the 5 mL pulse of H_2S. The values of C_x and C_a resulting in an homogeneous biofilm description and the reference value of k_S obtained from Mora et al. [3] were used to perform the sensitivity analysis. Results obtained from the sensitivity analysis are shown in Table 2.

The DO concentration in the liquid phase and within biofilm exhibited a remarkable sensitivity to all parameters tested. The most sensitive parameter was the kinetic constant for elemental sulfur oxidation (k_S), since DO concentration is highly dependent on consumption rates. These results indicated that elemental sulfur production and accumulation plays a major role as an intermediate compound and should be included and described adequately through the kinetic model. Sulfide oxidation rate can be diminished by excessive elemental sulfur accumulation, which is directly influenced by the rate during which elemental sulfur is consumed (k_S). On the other hand, parameters related to density and activity distribution within biofilm also showed an influence on the output variable. The high sensitivity values obtained for the parameters associated with the description of the biofilm heterogeneity, highlights the importance of the incorporation of this assumption into the mathematical model. Since the other parameters are either known experimentally or bibliographically referenced, the three parameters proposed for model calibration were the parameters related to the characterization of the biofilm heterogeneity (C_x,C_a, k_s).

4.4.3. Model calibration

The mathematical model was calibrated using the experimental data from period IV, corresponding to a substrate pulse of 5 mL. The estimated parameters during the calibration step are shown in Table 3. Discussion about C_x and C_a values with respect to

492 literature could not be performed since this is the first time that these parameters have
493 been included in biofilm modeling to describe heterogeneous structure and activity. In
494 this sense, a discussion about biofilm density and activity distribution calculated from
495 calibration results is presented in section 4.4.4. The estimated value for k_s lied within the
496 typical range reported in the literature that is between 0.833 and 0.030 g $S^{1/3}$ $g^{-1/3}$ VSS.

497 In Fig. 4, the predicted and experimental oxygen profiles in the gas, liquid and biofilm
498 phases after model calibration are shown. The agreement between experimental DO
499 concentration profiles and model estimations was evaluated through the normalized root
500 mean square error (NRMSE). The NRMSE calculated for DO concentration profiles in
501 gas and liquid phases, and within biofilm are presented in Table 4. Simulated oxygen
502 profiles in liquid and gas phases predicted accurately (NRMSE<10%) the experimentally
503 observed trends (Fig. 4a). Differences between experimental and simulated oxygen
504 evolution in the gas phase were smaller, considering a heterogeneous biofilm (Fig. 4a)
505 than considering a homogeneous biofilm (Fig. 3a). In the same way, heterogeneous
506 biofilm modeling also allowed an accurate simulation of the DO concentration in the
507 liquid phase. Although slight differences could be observed in the initial slope, a similar
508 DO concentration profile was predicted during H_2S consumption (between 100 and 450
509 s) and at the steady-state (after 450 s). The model also described satisfactorily the
510 experimental oxygen distribution within the biofilm for DO concentrations above the DO
511 detection limit of the microsensors (0.05 mg DO L^{-1}). Thus, the mathematical model
512 developed in this work provided a better simulation of DO distribution within the biofilm,
513 under H_2S oxidation conditions, compared with modeling the biofilm as a homogeneous
514 layer. These results highlighted that the addition of a heterogeneous biofilm description
515 in trickled beds modeling, such as that found in a BTF or in the heterogeneous
516 respirometer, improves biological activity description as well as the description of gas
517 and liquid phase dynamics.

518 **4.4.4. Prediction of selected model variables**

519 H_2S, sulfate and elemental sulfur concentrations were also model variables not
520 monitored on-line but estimated by the model. H_2S and sulfate concentration evolution in
521 the liquid phase and within the biofilm are shown in Fig. 5. Elemental sulfur concentration
522 within the biofilm is presented in Fig. 6a. Complementarily, biofilm density and activity
523 distribution are shown in Fig. 6b.

Simulated H_2S profiles showed that 3360 ppm_v of H_2S were depleted both in the gas and in the liquid phase 200 s after its injection (Fig. 5a). The H_2S within the first biofilm layer was also consumed during the first 200 s and kept close to zero for the inner layers during all the simulated period (Fig. 5b). The evolution of simulated H_2S concentration proved a low mass transport resistance at the liquid-biofilm interface. Therefore, it can be concluded that the biological oxidation capacity of the system was only limited by oxygen liquid-biofilm mass transport rate. This is confirmed by elemental sulfur production during H_2S biological oxidation. Elemental sulfur was produced as an intermediate during H_2S oxidation and was totally consumed before 200 s, except in the inner layers of the biofilm where limiting-oxygen conditions caused the accumulation of a small amount of sulfur until practically the end of the simulated period. In this sense, until 600 and 800 s, elemental sulfur was not totally depleted at a depth of 500 and 625 μm, respectively. Considering that sulfate was the final product of the oxidation, the sulfate concentration profile in the bulk liquid phase (Fig. 5c) exhibited a progressive step-like concentration increase caused by the oxidation of H_2S injected in the pulse and the elemental sulfur generated as intermediate. Sulfate was only produced after 100 s of simulating time when the elemental sulfur produced as the first oxidation product started to be oxidized (Fig. 6a). Sulfate concentration reached its final concentration at around t=400 s when H_2S oxidation was finished and all the elemental sulfur produced was completely oxidized. Insignificant differences were found between the simulated sulfate concentration (629 mg S L^{-1}) and the measured sulfate concentration in the liquid phase after the initial pulse (639 mg S L^{-1}). As shown in Fig. 5d, high mass transport rates helped to homogenize sulfate profiles within the biofilm. In this sense, although different sulfate production rates were obtained at the beginning of the simulated period, until 200 s, the same concentration was reached in all simulated depths at the steady state (after 400 s).

The spatial distribution of biofilm properties was also assessed. The simulation results presented in Fig. 6b confirmed that the cell density increased in the deeper layers of the biofilm. Results indicated that the biofilm density increased 14% along with the biofilm depth, from 3205 at the biofilm surface to 4430 g VSS L^{-1} deeper on. This trend is in agreement with experimental determinations in biofilms systems presented in Zhang and Bishop [51]. The increase in cell density results in a decrease in the biofilm porosity and, consequently, in a lower dispersion rate of chemicals within the biofilm. In this case, the relative dispersion coefficient (D_r) from the surface to the inner parts of the biofilm varied

between 0.31 and 0.26, respectively. Such 14% decrease in the dispersion coefficient within the biofilm was consistent with the mass transport rate distribution experimentally determined [36,52]. In the same way, several works have suggested a stratification in the biofilm activity, but conventional monitoring tools have not allowed to check and quantify activity gradients through biofilm layers. Remarkably, monitoring tools presented herein allowed estimating a distribution of the biological activity through the biofilm in the trickled bed. The calibration results showed a gradient in the fraction of active bacteria within the biofilm, which decreased from 0.95 to 0.45 along a biofilm section (Fig. 6b). These results are in high agreement with results presented in Zhang and Bishop [46] where a viable bacteria decrease from 91 to 39% was detected. In Mirpuri et al. [48] a qualitative explanation of the physiological biofilms stratification was proposed considering three categories of bacteria: those capable of degrading pollutants at high concentrations, those that can degrade pollutants at a low concentration under favorable conditions and those that cannot degrade pollutants at all. Experimental determinations indicated that the pollutants degrader bacteria are abundant near the liquid-biofilm interface while the other types are abundant deeper in the biofilm.

5. CONCLUSIONS

Coupling heterogeneous respirometry and DO microsensor specifically designed for biofilm profiling provided a complete tool for the characterization of biofiltration systems from a comprehensive monitoring through gas, liquid and biofilm phases. The improved heterogeneous respirometer exhibited a high performance for the study of multiphase processes taking place in packed bed systems such as biotrickling filters. Coupling experimental gas, liquid and biofilm data with a biofiltration model considering biofilm structural and functional heterogeneity, resulted in a complete characterization of the system. Mass transport and biokinetic mechanisms description were achieved from results obtained in the current study. To the best of our knowledge, this is the first work where a trickled bed is modeled as a 2D stratified system including experimental data from biofilm profiling. Results obtained allows deepening in the knowledge of biofilm processes and structure as well as improving the description provided by biofilm models.

6. ACKNOWLEDGEMENTS

The authors are members of the unit of Biochemical Engineering of Xarxa de Referència en Biotecnologia de Catalunya (XRB), Generalitat de Catalunya. Authors acknowledge the Spanish Government for providing funding through the projects RTI2018-099362-B-C21 MINECO/FEDER, EU and RTI2018-099362-B-C22 MINECO/FEDER, EU.

7. REFERENCES

[1] M.-C. Delhoménie, M. Heitz, Biofiltration of air: a review., Crit. Rev. Biotechnol. 25 (2005) 53–72. doi:10.1080/07388550590935814.

[2] L.R. López, a. D. Dorado, M. Mora, X. Gamisans, J. Lafuente, D. Gabriel, Modeling an aerobic biotrickling filter for biogas desulfurization through a multi-step oxidation mechanism, Chem. Eng. J. 294 (2016) 447–457. doi:10.1016/j.cej.2016.03.013.

[3] M. Mora, L.R. López, J. Lafuente, J. Pérez, R. Kleerebezem, M.C.M. van Loosdrecht, X. Gamisans, D. Gabriel, Respirometric characterization of aerobic sulfide, thiosulfate and elemental sulfur oxidation by S-oxidizing biomass, Water Res. 89 (2016) 282–292. doi:10.1016/j.watres.2015.11.061.

[4] L. Sgier, R. Freimann, A. Zupanic, A. Kroll, Flow cytometry combined with viSNE for the analysis of microbial biofilms and detection of microplastics, Nat. Commun. 7 (2016). doi:10.1038/ncomms11587.

[5] P.L. Bishop, Biofilm structure and kinetics, Water Sci. Technol. 36 (1997) 287–294.

[6] X. Guimerà, A.D. Dorado, A. Bonsfills, G. Gabriel, D. Gabriel, X. Gamisans, Dynamic characterization of external and internal mass transport in heterotrophic biofilms from microsensors measurements, Water Res. 102 (2016) 551–560. doi:10.1016/j.watres.2016.07.009.

[7] M. Piculell, T. Welander, K. Joñsson, Organic removal activity in biofilm and suspended biomass fractions of MBBR systems, Water Sci. Technol. 69 (2014) 55–61. doi:10.2166/wst.2013.552.

[8] R. Ramirez-Vargas, A. Ordaz, M. Carrión, I.Y. Hernández-Paniagua, F. Thalasso, Comparison of static and dynamic respirometry for the determination of stoichiometric and kinetic parameters of a nitrifying process, Biodegradation. 24 (2013) 675–684. doi:10.1007/s10532-012-9615-0.

[9] T.C. Zhang, P.L. Bishop, Experimental determination of the dissolved oxygen boundary layer and mass transfer resistance near the fluid-biofilm interface, Water Sci. Technol. 30 (1995) 47–58.

[10] S. Matsumoto, M. Katoku, G. Saeki, A. Terada, Y. Aoi, S. Tsuneda, C. Picioreanu, M.C.M. Van Loosdrecht, Microbial community structure in autotrophic nitrifying granules characterized by experimental and simulation analyses, Environ. Microbiol. 12 (2010) 192–206. doi:10.1111/j.1462-2920.2009.02060.x.

[11] T.P.W. Vannecke, G. Wells, N. Hubaux, E. Morgenroth, E.I.P. Volcke, Considering microbial and aggregate heterogeneity in biofilm reactor models: How far do we need to go?, Water Sci. Technol. 72 (2015) 1692–1699. doi:10.2166/wst.2015.389.

[12] J. Guo, Y. Peng, L. Fan, L. Zhang, B.J. Ni, B. Kartal, X. Feng, M.S.M. Jetten, Z. Yuan, Metagenomic analysis of anammox communities in three different microbial aggregates, Environ. Microbiol. 18 (2016) 2979–2993. doi:10.1111/1462-2920.13132.

[13] T. Smith-Palmer, S. Lin, I. Oguejiofor, T. Leng, A. Pustam, J. Yang, L.L. Graham, R.C. Wyeth, C.D. Bishop, M.E. Demont, D. Pink, In Situ Confocal Raman Microscopy of Hydrated Early Stages of Bacterial Biofilm Formation on Various Surfaces in a Flow Cell, Appl. Spectrosc. 70 (2016) 289–301. doi:10.1177/0003702815620539.

[14] P.S. Stewart, R. Murga, R. Srinivasan, D. de Beer, Biofilm structural heterogeneity visualized by three microscopic methods, Water Res. 29 (1995) 2006–2009. doi:10.1016/0043-1354(94)00339-9.

[15] S. Langer, D. Schropp, F.R. Bengelsdorf, M. Othman, M. Kazda, Dynamics of biofilm formation during anaerobic digestion of organic waste, Anaerobe. 29 (2014) 44–51. doi:10.1016/j.anaerobe.2013.11.013.

[16] S. Kim, M.A. Deshusses, Development and Experimental Validation of a Conceptual Model for Biotrickhg Ffltration of H2S, Environ. Prog. 22 (2003) 119–128.

[17] A.D. Dorado, G. Baquerizo, J.P. Maestre, X. Gamisans, D. Gabriel, J. Lafuente, Modeling of a bacterial and fungal biofilter applied to toluene abatement: Kinetic parameters estimation and model validation, Chem. Eng. J. 140 (2008) 52–61. doi:10.1016/j.cej.2007.09.004.

[18] D. De Beer, P. Stoodley, F. Roe, Z. Lewandowski, Effects of biofilm structures on oxygen distribution and mass transport, Biotechnol. Bioeng. 43 (1994) 1131–1138. doi:10.1002/bit.260431118.

[19] P.L. Bishop, T.C. Zhang, Y.-C. Fu, Effects of biofilm structure, microbial distributions and mass transport on biodegradation processes, Water Sci. Technol. 31 (1995) 143–152.

[20] X. Zhu, M.T. Suidan, C. Alonso, T. Yu, B.J. Kim, B.R. Kim, Biofilm structure and mass transfer in a gas phase trickle-bed biofilter, Water Sci. Technol. 43 (2001) 285–293.

[21] L. Fan, K.D. Wisecarver, B.J. Zehner, Diffusion of Phenol through a Biofilm Grown on Activated Carbon Particles in a Bioreactor, Biotechnol. Bioeng. 35 (1990) 279–286.

[22] T.C. Zhang, P.L. Bishop, Structure, activity and composition of biofilms, Water Sci. Technol. 29 (1994) 335–344.

[23] R.K. Hinson, W.M. Kocher, Model for effective diffusivities in aerobic biofilms, J. Environ. Eng. 122 (1996) 1023–1030.

[24] H. Horn, E. Morgenroth, Transport of oxygen, sodium chloride, and sodium nitrate

in biofilms, Chem. Eng. Sci. 61 (2006) 1347–1356. doi:10.1016/j.ces.2005.08.027.

[25] H. Beyenal, S. Seker, A. Tanyolaç, Diffusion Coefficients of Phenol and Oxygen in a Biofilm of Pseudomonas putida, AIChE J. 43 (1997) 243–250.

[26] F. Jiang, D.H. wai Leung, S. Li, G.H. Chen, S. Okabe, M.C.M. van Loosdrecht, A biofilm model for prediction of pollutant transformation in sewers, Water Res. 43 (2009) 3187–3198. doi:10.1016/j.watres.2009.04.043.

[27] A. González-Sánchez, L. Arellano-García, W. Bonilla-Blancas, G. Baquerizo, S. Hernández, D. Gabriel, S. Revah, Kinetic characterization by respirometry of volatile organic compound-degrading biofilms from gas-phase biological filters, Ind. Eng. Chem. Res. 53 (2014) 19405–19415. doi:10.1021/ie503327f.

[28] W. Bonilla-Blancas, M. Mora, S. Revah, J.A. Baeza, J. Lafuente, X. Gamisans, D. Gabriel, A. González-Sánchez, Application of a novel respirometric methodology to characterize mass transfer and activity of H2S-oxidizing biofilms in biotrickling filter beds, Biochem. Eng. J. 99 (2015) 24–34. doi:10.1016/j.bej.2015.02.030.

[29] D. De Beer, J.C. Van den Heuvel, S.P.P. Ottengraf, Microelectrode measurements of the activity distribution in nitrifying bacterial aggregates, Appl. Environ. Microbiol. 59 (1993) 573–579.

[30] V. Lazarova, J. Manem, Biofilm characterization and activity analysis in water and wastewater treatment, Water Res. 29 (1995) 2227–2245.

[31] C.M. Santegoeds, A. Schramm, D. De Beer, Microsensors as a tool to determine chemical microgradients and bacterial activity in wastewater biofilms and flocs., Biodegradation. 9 (1998) 159–167. doi:Doi 10.1023/A:1008302622946.

[32] H. Beyenal, Z. Lewandowski, Combined effect of substrate concentration and flow velocity on effective diffusivity in biofilms, Water Res. 34 (2000) 528–538. doi:10.1016/S0043-1354(99)00147-5.

[33] X.-H. Zhou, J. Liu, H.-M. Song, Y.-Q. Qiu, H.-C. Shi, Estimation of Heterotrophic Biokinetic Parameters in Wastewater Biofilms from Oxygen Concentration Profiles by Microelectrode, Environ. Eng. Sci. 29 (2012) 466–471. doi:10.1089/ees.2010.0456.

[34] A. Moya, X. Guimerà, F.J. del Campo, E. Prats-Alfonso, A.D. Dorado, M. Baeza, R. Villa, D. Gabriel, X. Gamisans, G. Gabriel, Profiling of oxygen in biofilms using individually addressable disk microelectrodes on a microfabricated needle, Microchim. Acta. 182 (2014) 985–993. doi:10.1007/s00604-014-1405-4.

[35] X. Guimerà, A. Moya, A.D. Dorado, X. Illa, R. Villa, D. Gabriel, X. Gamisan, G. Gabriel, A minimally invasive microsensor specially designed for simultaneous dissolved oxygen and pH biofilm profiling, Sensors (Switzerland). 19 (2019). doi:10.3390/s19214747.

[36] X. Guimerà, A. Moya, A.D. Dorado, R. Villa, D. Gabriel, G. Gabriel, X. Gamisans, Biofilm dynamics characterization using a novel DO-MEA sensor: mass transport and biokinetics., Appl. Microbiol. Biotechnol. (2014). doi:10.1007/s00253-014-5821-5.

[37] S.Y. Tan, T. Yu, H.C. Shi, Microsensor determination of multiple microbial processes in an oxygen-based membrane aerated biofilm, Water Sci. Technol. 69

(2014) 909–914. doi:10.2166/wst.2013.730.

[38] M. Kuhl, B.B. Jorgensen, Microsensor measurements of sulfate reduction and sulfide oxidation in compact microbial communities of aerobic biofilms, Appl. Environ. Microbiol. 58 (1992) 1164–1174.

[39] K. Jensen, N.P. Sloth, N. Risgaard-Petersen, S. Rysgaard, N.P. Revsbech, Estimation of nitrification and denitrification from microprofiles of oxygen and nitrate in model sediment systems., Appl. Environ. Microbiol. 60 (1994) 2094–2100. doi:papers2://publication/uuid/7FF0C1FF-3E04-4930-84BD-DCEB6465E720.

[40] H. Satoh, M. Odagiri, T. Ito, S. Okabe, Microbial community structures and in situ sulfate-reducing and sulfur-oxidizing activities in biofilms developed on mortar specimens in a corroded sewer system, Water Res. 43 (2009) 4729–4739.

[41] L. López De León, Development and application of control strategies in an aerobic biotrickling filter for H2S removal from biogas streams: experimental and modelling study, 2016.

[42] M. Fortuny, J.A. Baeza, X. Gamisans, C. Casas, J. Lafuente, M.A. Deshusses, D. Gabriel, Biological sweetening of energy gases mimics in biotrickling filters., Chemosphere. 71 (2008) 10–7. doi:10.1016/j.chemosphere.2007.10.072.

[43] A. Guisasola, Modelling biological organic matter and nutrient removal processes from wastewater using respirometric and titrimetric techniques, 2005.

[44] J. Roels, Energetics and kinetics in biotechnology, Elsevier Biomedical Press, 1983.

[45] APHA, Standard methods for the examination of water and wastewater, Edition 20, APHA/AWWA/WPCF, Washington DC, 1998.

[46] R. Billet, M. Schultes, Predicting mass transfer in packed columns, Chem. Eng. Technol. 16 (1993) 1–9. doi:10.1002/ceat.270160102.

[47] C. Van der Heyden, B. Vanthillo, J.G. Pieters, P. Demeyer, E.I.P. Volcke, Mechanistic Modeling of Pollutant Removal, Temperature, and Evaporation in Chemical Air Scrubbers, Chem. Eng. Technol. 39 (2016) 1785–1796. doi:10.1002/ceat.201500664.

[48] R.H. Perry, D.W. Green, Perry's chemical engineer's handbook, 7 Edition, Mc Graw-Hill, 1997.

[49] R. Sander, Compilation of Henry's law constants (version 4.0) for water as solvent, Atmos. Chem. Phys. 15 (2015) 4399–4981. doi:10.5194/acp-15-4399-2015.

[50] G. Trejo-Aguilar, S. Revah, R. Lobo-Oehmichen, Hydrodynamic characterization of a trickle bed air biofilter, Chem. Eng. J. 113 (2005) 145–152. doi:10.1016/j.cej.2005.04.001.

[51] T.C. Zhang, P.L. Bishop, Density, porosity, and pore structure of biofilms, Water Res. 28 (1994) 2267–2277. doi:10.1016/0043-1354(94)90042-6.

[52] H. Beyenal, Z. Lewandowski, G. Harkin, Quantifying biofilm structure: facts and fictions, Biofouling. 20 (2004) 1–23.

[53] R. Mirpuri, W. Sharp, S. Villaverde, W. Jones, Z. Lewandowski, A. Cunningham, Predictive model for toluene degradation and microbial phenotypic profiles in flat plate vapor phase bioreactor, J. Environ. Eng. 123 (1997) 586–592. doi:10.1061/(ASCE)0733-9372(1997)123:6(586).

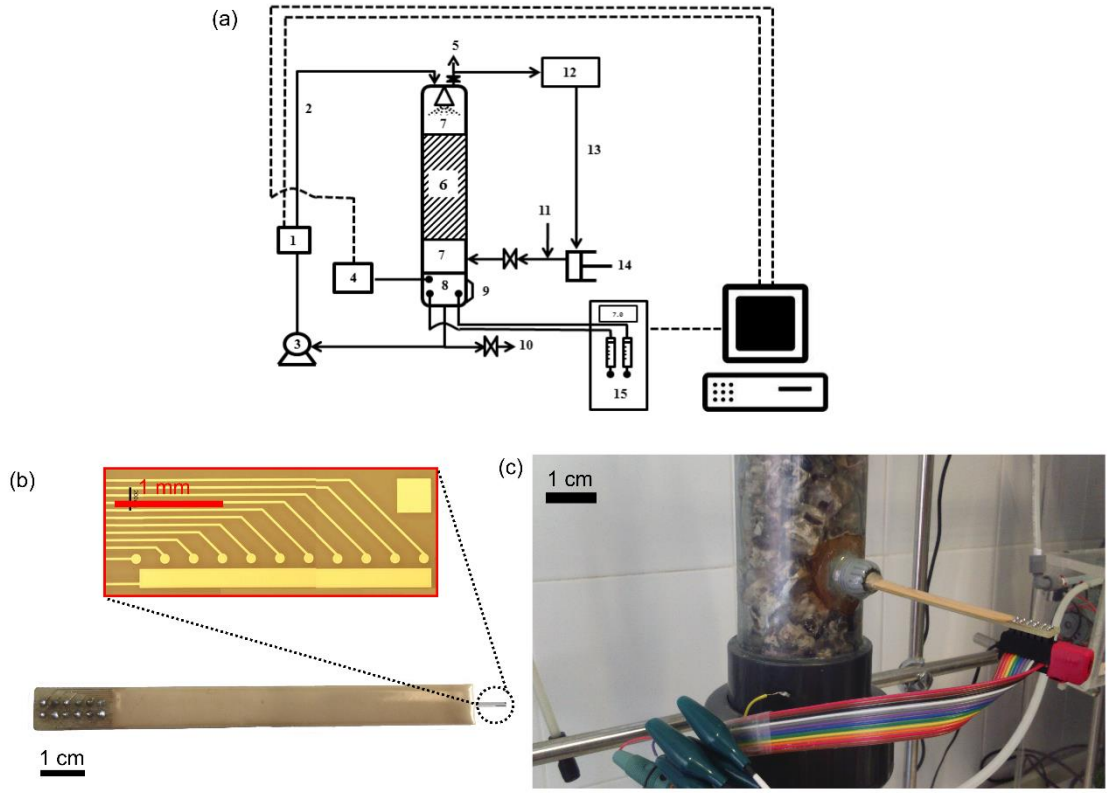

Fig. 1. (a) Schematic of the heterogeneous respirometer. 1. dissolved oxygen sensor, 2. liquid recirculation line, 3. liquid recirculation pump, 4. pH sensor, 5. gas out, 6. packed bed container, 7. free gas (gas volume not contained in the packed bed), 8. liquid reservoir, 9. pulse port, 10. liquid purge, 11. gas in, 12. O_2 sensor, 13. gas recirculation line, 14. gas recirculation compressor, 15. micro-burette for pH control; (b) DO microsensor; (c) detailed image of the biofilm monitoring port with the DO-MEA installed.

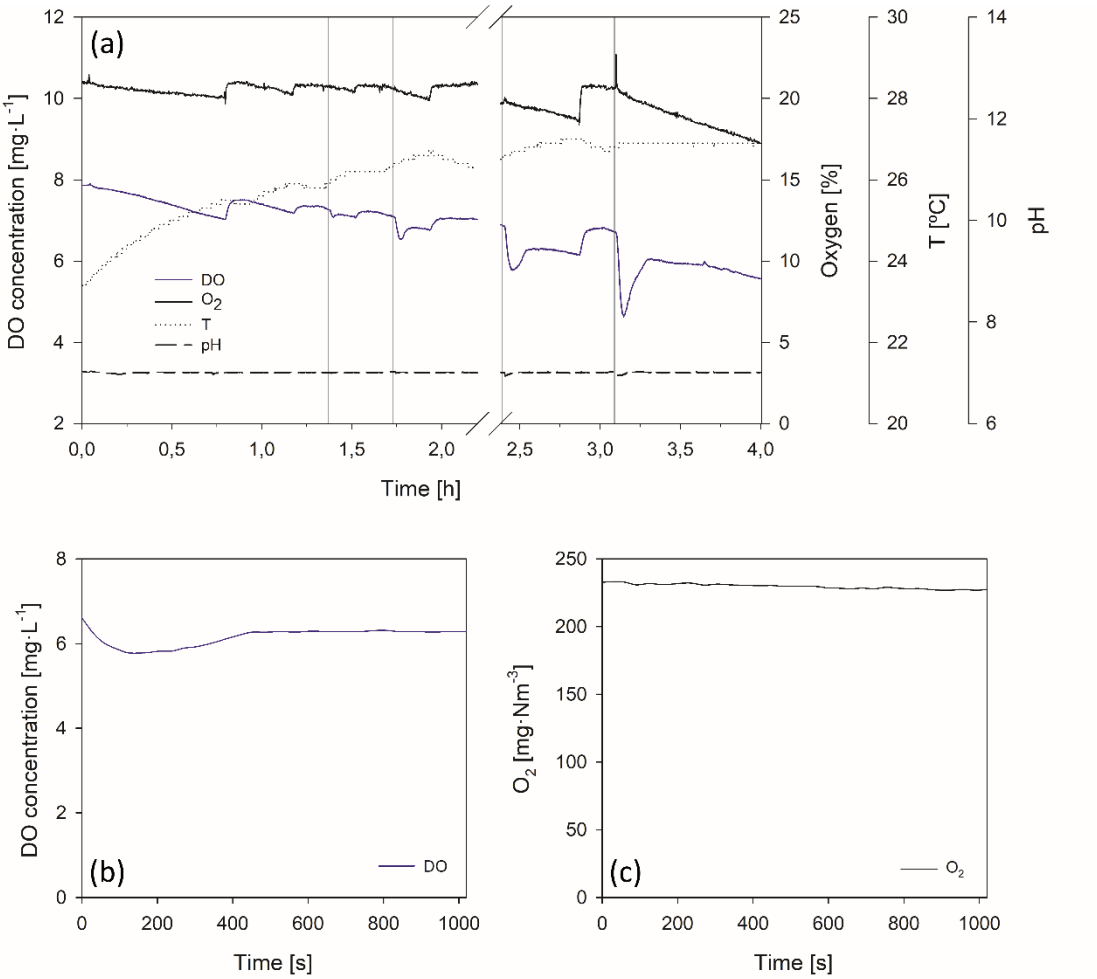

769

770 **Fig. 2.** (a) Respirometric profiles obtained from oxygen monitoring in gas and liquid phases
771 during the endogenous stage and during pulses of 200 µL (135 ppm_v), 1 mL (675 ppm_v), 5 mL
772 (3360 ppm_v) and 10 mL (6720 ppm_v) of H_2S. Vertical lines show the instant of pulses injection.
773 Oxygen concentration profile in the liquid phase (b) and gas phase (c) during the oxidation of
774 3360 ppm_v of H_2S.

775

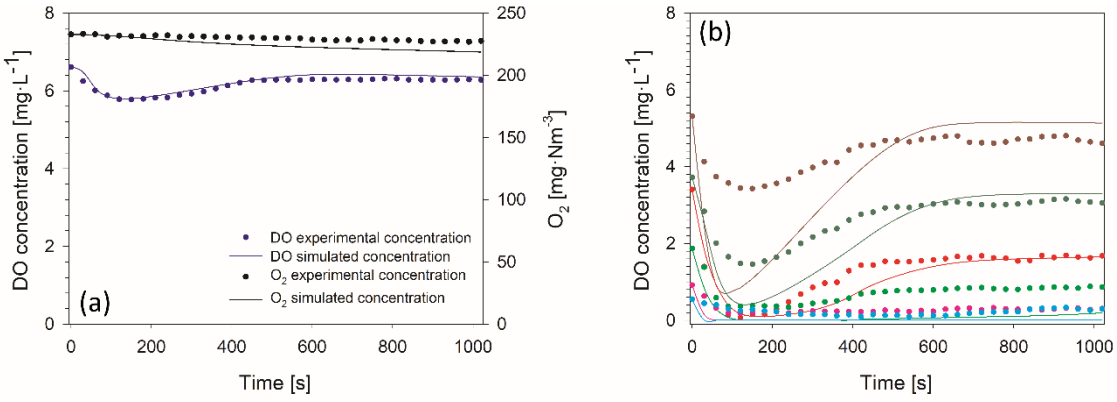

776

777 **Fig. 3.** Experimental (symbols) and simulated (solid lines) oxygen concentration profiles during
778 the 5 mL H_2S pulse considering a homogeneous biofilm (constant density and biomass activity)
779 in (a) the liquid and gas phases and (b) within the biofilm. Monitored depths are plotted in

different colors: brown (30 μm depth), green (155 μm depth), red (280 μm depth), light green (405 μm depth), purple (530 μm depth) and light blue (655 μm depth).

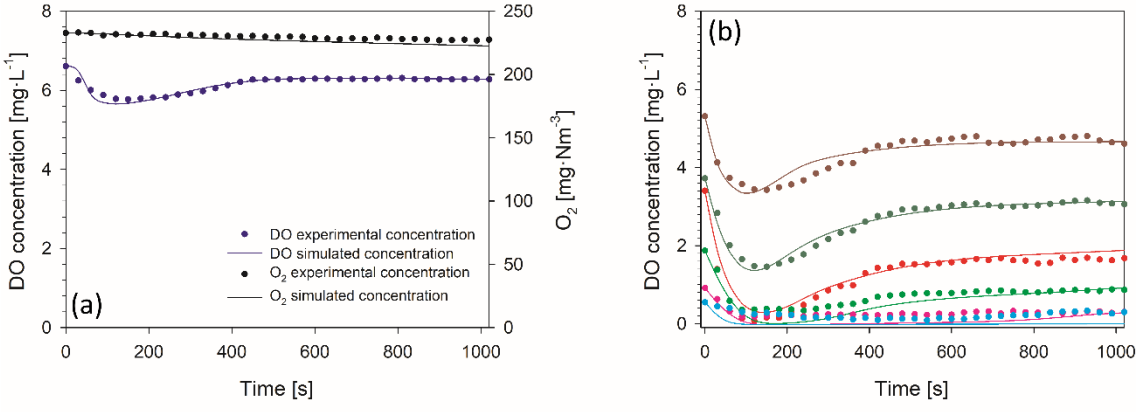

Fig. 4. Experimental (symbols) and simulated (solid lines) DO profiles in (a) gas and liquid phases and (b) within biofilm, used in model calibration. Profiles correspond to the 5 mL of H_2S. Monitored depths are plotted in different colors: brown (30 μm depth), green (155 μm depth), red (280 μm depth), light green (405 μm depth), purple (530 μm depth) and light blue (655 μm depth).

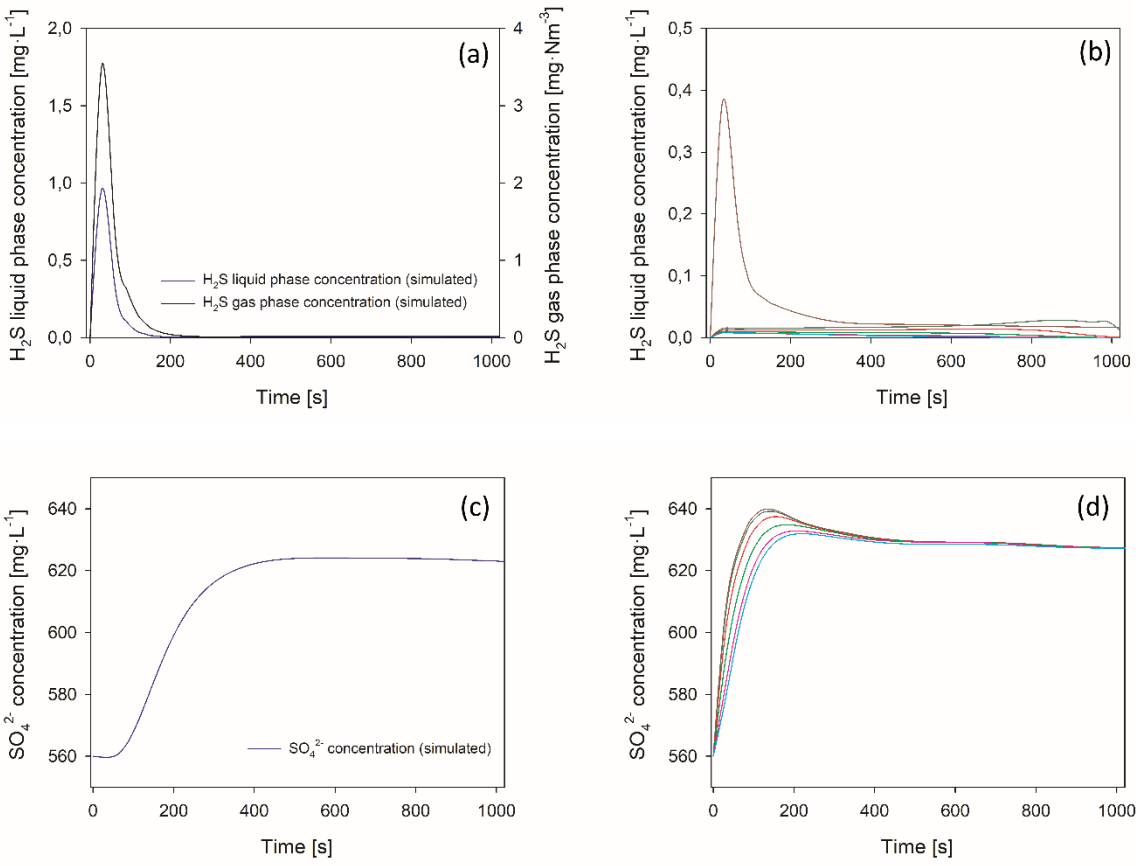

Fig. 5. Simulated H_2S in the (a) gas and liquid phase and (b) within the biofilm, sulfate concentration in the liquid phase (c) and within 6 simulated biofilm depths (d) during a pulse of 5 mL of H_2S. Monitored depths are plotted in different colors: brown (30 μm depth), green (155

μm depth), red (280 μm depth), light green (405 μm depth), purple (530 μm depth) and light blue (655 μm depth).

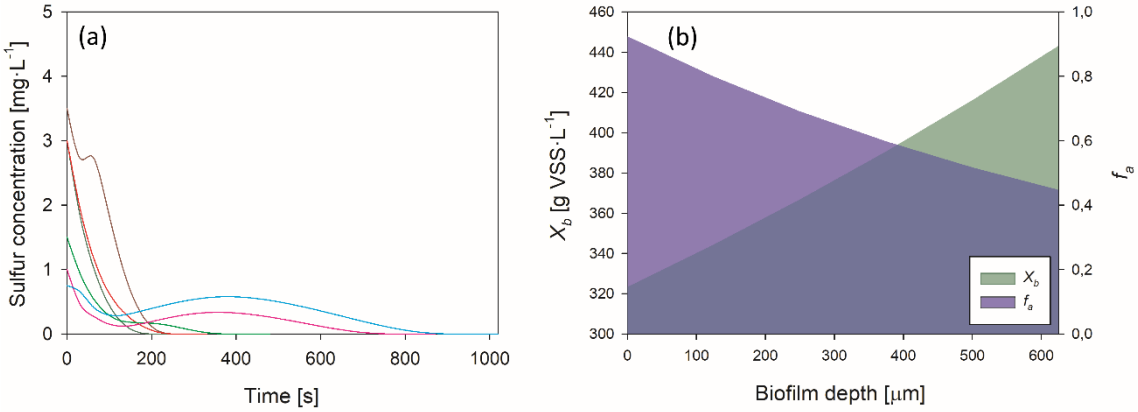

Fig. 6. (a) Simulated elemental sulfur concentration within 6 simulated biofilm depths during a pulse of 5 mL of H_2S. Monitored depths are plotted in different colours: brown (30 μm depth), green (155 μm depth), red (280 μm depth), light green (405 μm depth), purple (530 μm depth) and light blue (655 μm depth). (b) Biofilm density and activity distribution within a biofilm section calculated from calibration results (Eq. 4 and Eq. 5).

Table 1. Parameters related to system specifications experimentally determined in the heterogeneous respirometer.

Parameter	Value	Units
V_L	$1.26 \cdot 10^{-4}$	m^3
V_G	$14.9 \cdot 10^{-4}$	m^3
V_{Bed}	$6.30 \cdot 10^{-4}$	m^3
Dynamic hold-up	$23.5 \cdot 10^{-6}$	m^3
Static hold-up	$17.7 \cdot 10^{-6}$	m^3
Biofilm amount	16.2	g TS[a]
ε_x	0.11	g bacteria g^{-1} TS
ε_L^{Bed}	0.065	m^3 liquid m^{-3} bed
ε_B^{Bed}	0.063	m^3 biofilm m^{-3} bed
ε_G^{Bed}	0.762	m^3 gas m^{-3} bed

	ε_S^{Bed}	0.110	m^3 material m^{-3} bed

[a]Total Solids (TS)

Table 2. Sensitivity results of DO in the liquid phase and within first biofilm layer to selected model parameters for the heterogeneous biofilm model assessed for the 5 mL H_2S pulse.

Parameter	Units	DO liquid phase		DO Biofilm	
		Sensitivity, +Δ10%	Sensitivity, -Δ10%	Sensitivity, +Δ10%	Sensitivity, -Δ10%
C_x	m^{-1}	0.148	0.137	0.358	0.391
C_a	m^{-1}	0.189	0.168	0.411	0.396
k_S	g $S^{1/3}$ $g^{-1/3}$ VSS	-2.599	-2.794	5.781	3.487

Table 3. Model parameters estimated and calculated from the fitting of the improved mathematical model to the experimental respirometric profiles.

Parameter	Value	Units
C_x	262.28	m^{-1}
C_a	821.98	m^{-1}
k_S	0.0731	g $S^{1/3}$ $g^{-1/3}$ VSS

Table 4. Normalized root mean square errors (NRMSE) between experimental DO concentration profiles and model simulations in the gas and liquid phase, and within biofilm.

DO concentration profile		NRMSE [%]
Gas phase		1.4
Liquid phase		1.1
Biofilm	30 µm	3.5
	155 µm	2.4
	280 µm	3.2
	405 µm	7.5

	530 µm	9.3
	655 µm	11.1

815